Water Oxidation

DOI: 10.1002/anie.200901279

Catalytic and Surface-Electrocatalytic Water Oxidation by Redox Mediator–Catalyst Assemblies**

*Javier J. Concepcion, Jonah W. Jurss, Paul G. Hoertz, and Thomas J. Meyer**

We recently described single-site catalysts for water oxidation that operate by a well-defined mechanism involving stepwise three-electron oxidation to high-oxidation-state oxo complexes $[Ru^{V}(tpy)(bpm)(O)]^{3+}$ and $[Ru^{V}(tpy)(bpz)(O)]^{3+}$ (tpy = 2,2′:6′,2″-terpyridine; bpm = 2,2′-bipyrimidine; bpz = 2,2′-bipyrazine).[1] Additional single-site ruthenium catalysts have been identified by Thummel et al. that may utilize a related mechanism.[2] These reactions appear to occur through key O···O bond forming steps and peroxido intermediates that are reminiscent of the proposed water oxidation mechanism in the oxygen evolving complex (OEC) of photosystem II (PSII)[3,4] and water oxidation by the blue ruthenium dimer *cis,cis*-$[(bpy)_2(H_2O)Ru^{III}ORu^{III}(OH_2)(bpy)_2]^{4+}$ (bpy = 2,2′-bipyridine).[5] We also reported that rates of cerium(IV)-catalyzed water oxidation by the blue dimer are greatly enhanced by added redox mediators, $[Ru(bpy)_2(LL)]^{2+}$ (LL = bpy, bpm, or bpz) and $[Ru(bpm)_3]^{2+}$.[6] Herein, we present stable, robust water oxidation catalysis based on assemblies containing both functions in solution, and notably in methylenephosphonate derivatives on electrode surfaces, for which turnovers of more than 28000 have been achieved.

The assemblies can be synthesized in two steps: 1) Reaction of $[Ru^{II}(bpy)_2Cl_2]\cdot 2H_2O$ with $[Ru^{II}(LLL)(bpm)Cl]^{+}$[7,8] in 1:1 EtOH:$H_2O$ (LLL = tpy or Mebimpy: 2,6-bis(1-methylbenzimidazol-2-yl)pyridine; structures in Figure 1a); 2) removal of the chloro ligand and chloride counter ions in the resulting ligand-bridged assemblies $[(bpy)_2Ru^{II}(bpm)Ru^{II}(LLL)Cl]Cl_3$ by reaction with neat HOTf (OTf^{-} = trifluoromethanesulfonate) followed by displacement of OTf^{-} in water to give $[(bpy)_2Ru^{II}(bpm)Ru^{II}(tpy)(OH_2)]^{4+}$ (**1**) or $[(bpy)_2Ru^{II}(bpm)Ru^{II}(Mebimpy)(OH_2)]^{4+}$ (**2**). Purification was achieved by column chromatography (Sephadex LH-20) by using water as the eluant.

The corresponding methylenephosphonate ethyl esther derivatives were prepared by similar strategies by replacing $[Ru^{II}(bpy)_2Cl_2]\cdot 2H_2O$ with $[\{[4,4'\text{-}(EtO)_2OPCH_2]_2bpy\}_2Ru^{II}Cl_2]$.[9] Hydrolysis of the methylenephosphonate ethyl esther derivatives in 4.0 M HCl gave the corresponding phosphonic acid derivatives, which were treated in a similar fashion with neat triflic acid and water to give $[\{[4,4'\text{-}(HO)_2OPCH_2]_2bpy\}_2Ru^{II}(bpm)Ru^{II}(tpy)(OH_2)]^{4+}$ (**1**-PO_3H_2) and $[\{[4,4'\text{-}(HO)_2OPCH_2]_2bpy\}_2Ru^{II}(bpm)Ru^{II}(Mebimpy)(OH_2)]^{4+}$ (**2**-PO_3H_2). Purification was also achieved by column chromatography on Sephadex LH-20 by using water as the eluant. Complexes **1** and **2** were characterized by ^{1}H NMR and UV/Vis spectroscopy, high-resolution mass spectrometry, and cyclic voltammetry, and **1**-(PO_3H_2) and **2**-(PO_3H_2) by ^{1}H NMR, ^{31}P NMR, and UV/Vis spectroscopy, cyclic voltammetry, and elemental analysis (CHNFS; see the Supporting Information).

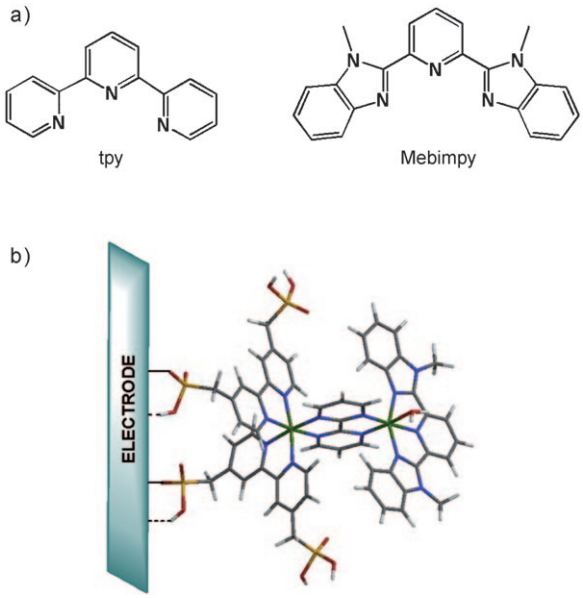

Figure 1. a) Structures of tpy and Mebimpy. b) Redox mediator–water oxidation catalyst assembly **2**-PO_3H_2 anchored to a metal oxide electrode. Ru green, N blue, O red, P yellow.

All four complexes have intense, pH-dependent MLCT absorptions in the visible region. The complexes are green in their aqua forms, $[\{4,4'\text{-}(X)_2bpy\}_2Ru^{II}(bpm)Ru^{II}(LLL)(OH_2)]^{4+}$, X = $(HO)_2OPCH_2$ or H. For $[(bpy)_2Ru_1^{II}(bpm)Ru_2^{II}(tpy)(OH_2)]^{4+}$, a $d\pi(Ru_2)\rightarrow\pi^*(bpm)$ absorption occurs at $\lambda_{max} = 610$ nm ($\varepsilon = 8800\ L\,mol^{-1}\,cm^{-1}$) and overlapping $d\pi(Ru_1,Ru_2)\rightarrow\pi^*(bpm)$, $d\pi(Ru_1)\rightarrow\pi^*(bpy)$, $d\pi(Ru_2)\rightarrow\pi^*(tpy)$ bands at 457 nm (shoulder, $\varepsilon = 13400\ L\,mol^{-1}\,cm^{-1}$) and 413 nm ($\varepsilon = 27300\ L\,mol^{-1}\,cm^{-1}$) at pH 1.

Complexes **1** and **2** both display multiple, pH-dependent oxidations in cyclic voltammograms in aqueous solutions. In 0.1 M HNO_3, **1** undergoes two one-electron oxidations at 0.92

[*] Dr. J. J. Concepcion, J. W. Jurss, Dr. P. G. Hoertz, Dr. T. J. Meyer
Department of Chemistry,
University of North Carolina at Chapel Hill
Chapel Hill, NC 27516 (USA)
Fax: (+1) 919-962-2388
E-mail: tjmeyer@unc.edu

[**] Funding support for this research by the Chemical Sciences, Geosciences and Biosciences Division of the Office of Basic Energy Sciences, U.S. Department of Energy through grant number DE-FG02-06ER15788 is gratefully acknowledged.

Supporting information for this article is available on the WWW under http://dx.doi.org/10.1002/anie.200901279.

and 1.30 V (vs NHE) as opposed to the two-electron oxidation of $[Ru(tpy)(bpm)(OH_2)]^{2+}$[1] [Equations (1) and (2)]. At higher potentials, $[Ru^{III}(bpm)Ru^{IV}{=}O]^{5+}/[Ru^{II}(bpm)Ru^{IV}{=}O]^{4+}$ (1.41 V) and $[Ru^{III}(bpm)Ru^{V}{=}O]^{6+}/[Ru^{III}(bpm)Ru^{IV}{=}O]^{5+}$ (1.69 V) waves are observed at the onset of a catalytic water oxidation wave [Equations (3) and (4)].

$$[(bpy)_2Ru^{II}(bpm)Ru^{II}(tpy)(OH_2)]^{4+} - H^+ - e^- \rightarrow [(bpy)_2Ru^{II}(bpm)Ru^{III}(tpy)(OH)]^{4+} \quad (1)$$

$$[(bpy)_2Ru^{II}(bpm)Ru^{III}(tpy)(OH)]^{4+} - H^+ - e^- \rightarrow [(bpy)_2Ru^{II}(bpm)Ru^{IV}(tpy)(O)]^{4+} \quad (2)$$

$$[(bpy)_2Ru^{II}(bpm)Ru^{IV}(tpy)(O)]^{4+} - e^- \rightarrow [(bpy)_2Ru^{III}(bpm)Ru^{IV}(tpy)(O)]^{5+} \quad (3)$$

$$[(bpy)_2Ru^{III}(bpm)Ru^{IV}(tpy)(O)]^{5+} - e^- \rightarrow [(bpy)_2Ru^{III}(bpm)Ru^{V}(tpy)(O)]^{6+} \quad (4)$$

For **2** at pH 1, there are also separate one-electron $Ru^{IV/III}$, $Ru^{III/II}$ waves at 1.30 V and 0.69 V vs. NHE, with the $Ru^{IV}{=}O/Ru^{III}$-OH couple of the catalytic site overlapping with the $Ru^{III/II}$ couple of the redox mediator at 1.33 V. The $Ru^{III/II}$ couple is followed by a $[Ru^{III}(bpm)Ru^{V}{=}O]^{6+}/[Ru^{III}(bpm)Ru^{IV}{=}O]^{5+}$ wave at the onset of a wave for catalytic water oxidation at 1.57 V.

Figure 2a shows a stopped-flow absorbance–time trace, which illustrates the appearance of a series of intermediates in the catalytic oxidation of water by **1**, and also a fit of the data to the kinetic model in Scheme 1. The results of a series of studies in 0.1 M HNO_3, including rate constants for individual steps, are summarized in Scheme 1, with spectra of intermediates shown in Figure 2b.

The steps a–h) in Scheme 1 can be summarized as follows: a,b) The initial oxidation of $[(bpy)_2Ru^{II}(bpm)Ru^{II}(tpy)(OH_2)]^{4+}$ ($[Ru_1^{II}Ru_2^{II}\text{-}OH_2]^{4+}$) to $[Ru_1^{II}Ru_2^{IV}{=}O]^{4+}$, which occurs with $k_1 = 2.1\times10^3\ L\,mol^{-1}\,s^{-1}$. The intermediate $[Ru^{II}Ru^{III}\text{-}OH]^{4+}$ does not build up in solution as it undergoes further rapid oxidation to $[Ru_1^{II}Ru_2^{IV}{=}O]^{4+}$. As shown by the green and red spectra in Figure 2b, formation of $[Ru_1^{II}Ru_2^{IV}{=}O]^{4+}$ is accompanied by loss of $Ru_2^{II}\rightarrow$tpy,bpy MLCT bands in the visible region. c) Oxidation of $[Ru_1^{II}Ru_2^{IV}{=}O]^{4+}$ to $[Ru_1^{III}Ru_2^{IV}{=}O]^{5+}$ ($k_2 = 390\ L\,mol^{-1}\,s^{-1}$) results in disappearance of $Ru_2^{II}\rightarrow$bpm,bpy MLCT bands and appearance of low absorptivity features in the visible region (Figure 2b). d) Oxidation of $[Ru^{III}Ru^{IV}O]^{5+}$ to $[Ru^{III}Ru^{V}{=}O]^{6+}$ ($k_3 = 104\ L\,mol^{-1}\,s^{-1}$) occurs with appearance of similar features, and probably arises from a combination of ligand-to-metal charge transfer (LMCT) and mixed valence absorptions.

The fate of $[Ru^{III}Ru^{V}{=}O]^{6+}$ depends on the concentration of cerium(IV). If generated stoichiometrically, by adding 4 equivalents of cerium(IV) to $[Ru^{II}Ru^{II}\text{-}OH_2]^{4+}$, it disappears by pseudo first order kinetics, with $k_{O-O} = 1.9\times10^{-3}\ s^{-1}$, to give $[Ru^{III}Ru^{III}\text{-}OOH]^{5+}$ as a discernible intermediate (e), analogous to $[Ru^{III}(tpy)(bpm)(OOH)]^{2+}$.[1] This is the key O···O bond-forming step. If generated in the presence of excess cerium(IV), $[Ru^{III}Ru^{III}\text{-}OOH]^{5+}$ is oxidized rapidly, presumably to $[Ru^{III}Ru^{IV}\text{-}OO]^{5+}$ (f). With excess cerium(IV), disappearance of $[Ru^{III}Ru^{IV}\text{-}OO]^{5+}$ becomes first order in

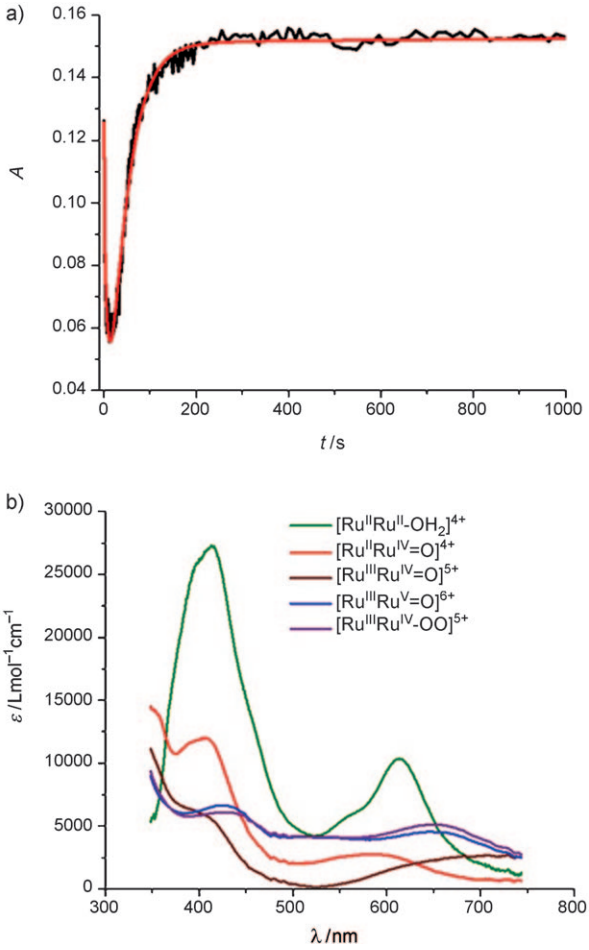

Figure 2. a) Absorbance–time trace (black curve) at 546 nm for **1** following addition of 10 equivalents of Ce^{IV} to $[(bpy)_2Ru^{II}(bpm)Ru^{II}(tpy)(OH_2)]^{4+}$ in 0.1 M HNO_3 at 298 K. The fit of the absorbance–time trace to the mechanism in Scheme 1 is shown (red) with $k_1 = 2.1\times10^3\ L\,mol^{-1}\,s^{-1}$; $k_2 = 390\ L\,mol^{-1}\,s^{-1}$; $k_3 = 104\ L\,mol^{-1}\,s^{-1}$; $k_{O-O} = 1.9\times10^{-3}\ s^{-1}$, and $k_4 = 40\ L\,mol^{-1}\,s^{-1}$. b) As in (a), spectra of intermediates obtained by stopped flow measurements, with spectral deconvolution during the course of the reaction.

$$Ru^{II}Ru^{II}\text{-}OH_2^{4+} + Ce^{4+} \xrightarrow{rapid} Ru^{II}Ru^{III}\text{-}OH^{4+} + Ce^{3+} + H^+ \quad (a)$$

$$Ru^{II}Ru^{III}\text{-}OH^{4+} + Ce^{4+} \xrightarrow{k_1} Ru^{II}Ru^{IV}{=}O^{4+} + Ce^{3+} + H^+ \quad (b)$$

$$Ru^{II}Ru^{IV}{=}O^{4+} + Ce^{4+} \xrightarrow{k_2} Ru^{III}Ru^{IV}{=}O^{5+} + Ce^{3+} \quad (c)$$

$$Ru^{III}Ru^{IV}{=}O^{5+} + Ce^{4+} \xrightarrow{k_3} Ru^{III}Ru^{V}{=}O^{6+} + Ce^{3+} \quad (d)$$

$$Ru^{III}Ru^{V}{=}O^{6+} + H_2O \xrightarrow{k_{O\text{-}O}} \{Ru^{III}Ru^{III}\text{-}O_2H\}^{5+} + H^+ \quad (e)$$

$$\{Ru^{III}Ru^{III}\text{-}O_2H\}^{5+} + Ce^{4+} \xrightarrow{rapid} Ru^{III}Ru^{IV}\text{-}O_2^{5+} + Ce^{3+} + H^+ \quad (f)$$

$$Ru^{III}Ru^{IV}\text{-}O_2^{5+} + Ce^{4+} \xrightarrow{k_4} \{Ru^{III}Ru^{V}\text{-}O_2\}^{6+} + Ce^{3+} \quad (g)$$

$$\{Ru^{III}Ru^{V}\text{-}O_2\}^{6+} + H_2O \xrightarrow{rapid} \{Ru^{III}Ru^{III}\text{-}OH\}^{5+} + O_2 + H^+ \quad (h)$$

Scheme 1. Reactions and rate constants for water oxidation by $[(bpy)_2Ru^{II}(bpm)Ru^{II}(tpy)(OH_2)]^{4+}$ in 0.1 M HNO_3 at 25 °C. Oxidation of $[Ru^{III}Ru^{IV}\text{-}O_2]^{5+}$ to $[Ru^{III}Ru^{V}\text{-}O_2]^{6+}$, Equation (g), is rate limiting, with $[Ru^{III}Ru^{IV}\text{-}O_2]^{5+}$ dominant at the catalytic steady state.

cerium(IV) and first order in $[Ru^{III}Ru^{IV}\text{-}OO]^{5+}$, with $k_4 = 40\ L\,mol^{-1}\,s^{-1}$. g,h) Further oxidation appears to give $[Ru^{III}Ru^{V}\text{-}OO]^{6+}$, which does not build up in solution as it undergoes rapid oxygen evolution to give $[Ru^{II}Ru^{IV}{=}O]^{4+}$, thus closing the catalytic cycle.

Under catalytic conditions with 30 equivalents of cerium(IV) added, the proposed Ru^{IV} peroxo intermediate $[(bpy)_2Ru^{III}(bpm)Ru^{IV}(LLL)(OO)]^{5+}$ dominates at the catalytic steady state. Loss of cerium(IV), monitored at 360 nm, is first order in cerium(IV) and first order in complex, with $k(25\,°C) = 40\ L\,mol^{-1}\,s^{-1}$ for $[(bpy)_2Ru^{II}(bpm)Ru^{II}(tpy)(OH_2)]^{4+}$ (**1**) and $60\ L\,mol^{-1}\,s^{-1}$ for $[(bpy)_2Ru^{II}(bpm)Ru^{II}(Mebimpy)(OH_2)]^{4+}$ (**2**). Assembly **2** utilizes an analogous mechanism, as shown by stopped flow measurements. Oxygen monitoring with an oxygen electrode in 0.1 M HNO_3 with 30 equivalents of cerium(IV) gave $100 \pm 3\,\%$ of the expected oxygen for circa 7.5 turnovers for both **1** and **2**.

The phosphonated versions of **1** and **2** can be anchored to metal oxide surfaces, such as tin-doped indium oxide (ITO) and fluorine-doped tin oxide (FTO), from acidic aqueous solutions (Figure 1b). Surface electrochemical behavior is similar to that for the non-phosphonated complexes in solution, with pH-dependent one-electron waves appearing for **1**-PO_3H_2 at $E_{1/2}$ ($Ru^{III}\text{-}OH_2/Ru^{II}\text{-}OH_2$) = 0.86 V and $E_{1/2}$ ($Ru^{IV}{=}O/Ru^{III}\text{-}OH_2$) = 1.20 V (1.0 M $HClO_4$), followed by a pH-dependent wave at 1.43 V (Ru^{III}/Ru^{II}-redox mediator). The pH-dependence for this wave is due to the presence of the phosphonate groups, as seen from the Pourbaix diagrams for **1**-PO_3H_2 and **2**-PO_3H_2 (Supporting Information). A pH-independent wave at 1.69 V ($Ru^{V}{=}O/Ru^{IV}{=}O$) appears at the onset of a catalytic water oxidation wave.

Electrolysis with **1**-PO_3H_2 or **2**-PO_3H_2 at 1.8 V vs NHE anchored to ITO in 1.0 M $HClO_4$ resulted in sustained, constant catalytic currents for more than 20 h, with no sign of decrease in catalytic activity. In one set of experiments (Figure 3), **1**-PO_3H_2 underwent 8900 turnovers with a turnover frequency (TOF) of 0.3 s^{-1}. Under similar conditions, **2**-PO_3H_2 underwent more than 28000 turnovers over a 13 hour period with a turnover rate of 0.6 s^{-1}, with no sign of reduction in catalytic activity.

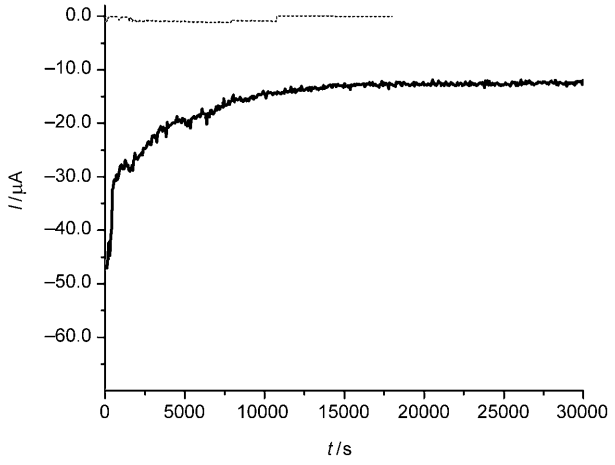

Figure 3. Electrolysis of **1**-PO_3H_2 anchored to ITO at 1.8 V in 1.0 M $HClO_4$. ••••• Background ITO; —— **1**-PO_3H_2. 8900 turnovers, TOF = 0.3 s^{-1}, current density $j \approx 6.7\ \mu A\,cm^{-2}$, $\Gamma \approx 7 \times 10^{-10}\ mol\,cm^{-2}$, $A = 1.95\ cm^2$.

Sustained electrocatalytic water oxidation is also observed for **1**-PO_3H_2 or **2**-PO_3H_2 anchored to circa 10 μm thick optically transparent films of nanoparticle TiO_2 (10–20 nm diameter) on FTO (FTO | TiO_2). Electrolysis of FTO | TiO_2 | **1**-PO_3H_2 ($\Gamma \approx 8.5 \times 10^{-8}\ mol\,cm^{-2}$, $A = 1.8\ cm^2$) at 1.8 V in 0.1 M HNO_3 for 30000 seconds yielded 12.6 μmol of O_2 with 4.99 coulombs of charged passed (12.9 μmol of expected oxygen; Supporting Information, Figure S7). This result corresponds to a Faradaic efficiency of circa 98 % for oxygen production. Electrolysis of FTO | TiO_2 | **2**-PO_3H_2 at 1.8 V gave similar results, with a Faradaic efficiency of circa 97 % for electrocatalytic water oxidation.

The impact of the redox mediator on water oxidation catalysis was demonstrated by holding the applied potential past the $Ru^{III/II}$ mediator wave at 1.43 V for **1**-PO_3H_2 and **2**-PO_3H_2 anchored to ITO in 0.1 M HNO_3 (Supporting Information, Figure S8). In both cases, sustained currents well above background were observed over extended periods. By comparison, under these conditions there is no electrocatalytic current for the related monomeric catalysts $[Ru(tpy)(bpm)(OH_2)]^{2+}$ or $[Ru(tpy)(bpz)(OH_2)]^{2+}$ in solution, thus demonstrating the importance of the mediator. Catalytic currents were lower than at 1.8 V, as expected, because surface oxidation to the reactive $Ru^{V}{=}O$ form, $[Ru_1^{III}\text{-}Ru_2^{IV}{=}O]^{5+} \rightarrow [Ru_1^{III}\text{-}Ru_2^{V}{=}O]^{5+}$, is disfavored by $\Delta G^{o\prime} \approx +0.26$ eV, thus slowing the overall rate of water oxidation.

These experiments are important in demonstrating the ability of the redox mediator to drive water oxidation at an adjacent catalytic site near the thermodynamic potential for the O_2/H_2O couple. This is a prerequisite, for example, in a dye-sensitized photoelectrochemical device in which the available potential is fixed at the potential of the surface site.

The robustness and turnover rates of these catalysts are encouraging. They oxidize water following single-site, well-defined mechanisms similar to those previously reported for $[Ru(tpy)(bpm)(OH_2)]^{2+}$ and $[Ru(tpy)(bpz)(OH_2)]^{2+}$[1] and offer promise in electrocatalytic and photoelectrocatalytic water oxidation.

Experimental Section

Detailed synthetic procedures are described in the Supporting Information. UV/Vis spectra were recorded on an Agilent Technologies Model 8453 diode-array spectrophotometer. Stopped-flow experiments were performed on a Hi-Tech SF-61 DX2 double mixing stopped-flow system equipped with a diode array detector. The stopped volume was 100 μL and the initial concentrations in the syringes of **1** and Ce^{IV} were 5×10^{-5} and 5×10^{-4} M, respectively. Kinetic measurements were also performed on a Shimadzu UV/Vis/NIR Spectrophotometer Model UV-3600 by monitoring the disappearance of Ce^{IV} at 360 nm. Data were processed by use of the program SPECFIT/32 Global Analysis System (SPECTRUM Software Associates). Electrochemical measurements were performed on an EG&G Princeton Applied Research model 273A potentiostat/galvanostat. Voltammetric measurements were made with a planar EG&G PARC G0229 glassy carbon millielectrode, a platinum wire EG&G PARC K0266 counter electrode, and Ag/AgCl EG&G PARC K0265 reference electrode. Oxygen measurements were performed with a calibrated O_2 electrode (YSI, Inc., Model 550A). In a typical

experiment, 30 equivalents of Ce^{IV} were added to stirred solutions containing 2.9×10^{-3} M **1** or **2** in 1.0 M HNO_3. The air-tight reaction cell was purged with argon prior to the addition of the Ce^{IV} until the digital readout had stabilized. O_2 evolution versus time was recorded and the theoretical maximum was achieved within 3%. Oxygen measurements for electrocatalytic water oxidation were performed with a fluorescence-based YSI ProODO O_2 calibrated electrode using an in-house built electrochemical cell.

Received: March 7, 2009
Revised: September 22, 2009
Published online: November 10, 2009

Keywords: electrocatalysis · redox chemistry · ruthenium · supported catalysts · water splitting

[1] J. J. Concepcion, J. W. Jurss, J. L. Templeton, T. J. Meyer, *J. Am. Chem. Soc.* **2008**, *130*, 16462 – 16463.
[2] H.-W. Tseng, R. Zong, J. T. Muckerman, R. Thummel, *Inorg. Chem.* **2008**, *47*, 11763 – 11773.
[3] T. J. Meyer, M. H. V. Huynh, H. H. Thorp, *Angew. Chem.* **2007**, *119*, 5378 – 5399; *Angew. Chem. Int. Ed.* **2007**, *46*, 5284 – 5304.
[4] G. Renger, *Photosynth. Res.* **2007**, *92*, 407 – 425.
[5] F. Liu, J. J. Concepcion, J. W. Jurss, T. Cardolaccia, J. L. Templeton, T. J. Meyer, *Inorg. Chem.* **2008**, *47*, 1727 – 1752.
[6] J. J. Concepcion, J. W. Jurss, J. L. Templeton, T. J. Meyer, *Proc. Natl. Acad. Sci. USA* **2008**, *105*, 17632 – 17635.
[7] K. J. Takeuchi, M. S. Thompson, D. W. Pipes, T. J. Meyer, *Inorg. Chem.* **1984**, *23*, 1845 – 1851.
[8] S. Swavey, Z. Fang, K. J. Brewer, *Inorg. Chem.* **2002**, *41*, 2598 – 2607.
[9] G. Will, G. Boschloo, S. N. Rao, D. Fitzmaurice, *J. Phys. Chem. B* **1999**, *103*, 8067 – 8079.

